Bioclickable and mussel adhesive peptide mimics for engineering vascular stent surfaces

Zhilu Yang[a,1], Xin Zhao[b,1], Rui Hao[a], Qiufen Tu[a], Xiaohua Tian[c], Yu Xiao[a], Kaiqing Xiong[a], Miao Wang[c], Yonghai Feng[c], Nan Huang[a,2], and Guoqing Pan[c,2]

[a]Key Laboratory of Advanced Technologies of Materials, Ministry of Education, School of Materials Science and Engineering, Southwest Jiaotong University, 610031 Chengdu, Sichuan, China; [b]Department of Biomedical Engineering, The Hong Kong Polytechnic University, Hung Hom, Hong Kong, China; and [c]Institute for Advanced Materials, School of Materials Science and Engineering, Jiangsu University, 212013 Zhenjiang, Jiangsu, China

Edited by David A. Weitz, Harvard University, Cambridge, MA, and approved May 28, 2020 (received for review February 27, 2020)

Thrombogenic reaction, aggressive smooth muscle cell (SMC) proliferation, and sluggish endothelial cell (EC) migration onto bioinert metal vascular stents make poststenting reendothelialization a dilemma. Here, we report an easy to perform, biomimetic surface engineering strategy for multiple functionalization of metal vascular stents. We first design and graft a clickable mussel-inspired peptide onto the stent surface via mussel-inspired adhesion. Then, two vasoactive moieties [i.e., the nitric-oxide (NO)-generating organoselenium (SeCA) and the endothelial progenitor cell (EPC)-targeting peptide (TPS)] are clicked onto the grafted surfaces via bioorthogonal conjugation. We optimize the blood and vascular cell compatibilities of the grafted surfaces through changing the SeCA/TPS feeding ratios. At the optimal ratio of 2:2, the surface-engineered stents demonstrate superior inhibition of thrombosis and SMC migration and proliferation, promotion of EPC recruitment, adhesion, and proliferation, as well as prevention of in-stent restenosis (ISR). Overall, our biomimetic surface engineering strategy represents a promising solution to address clinical complications of cardiovascular stents and other blood-contacting metal materials.

mussel adhesive peptide | vascular stents | surface bioengineering | NO generation | EPC capture

Since the first vascular endoprosthesis developed for relieving arterial obstruction in 1987 (1), vascular stent implantation has become the central therapy to treat cardiovascular diseases in clinics (2). The popularity of stenting is owing to the immediate effects of considerably reducing acute vessel closure. However, the long-term clinical success of stenting is limited due to complications such as in-stent restenosis (ISR, i.e., thrombosis and intimal hyperplasia at the interfaces of vascular implants) (3–8). ISR occurs when endothelium is damaged by stenting, which provokes prothrombogenic reactions, triggers platelet adhesion, aggregation and activation on the metal stents, and narrows the stented coronary artery considerably. This may eventually result in failure of vascular stents, and other complications including sudden death or nonfatal myocardial infarction (9, 10). The damages of endothelium will also trigger excessive smooth muscle cell (SMC) migration from vascular middle membrane and proliferation at the lesion (i.e., intimal hyperplasia). Accompanied by extracellular matrix deposition, such events lead to eventually ISR (11, 12). Hence, platelet and SMC suppression are essential for combating ISR.

Earlier strategies for ISR prevention rarely considered endothelial regeneration. For instance, drug-eluting stents are effective in reducing early thrombosis and inflammation, as well as inhibiting SMC migration and proliferation. However, the delayed vascular and especially endothelial healing usually result in high risk of late stent thrombosis and ISR (13). Later, another strategy, known as in vitro endothelialization, was developed by preseeding endothelial cells (ECs) onto vascular device surfaces prior to implantation (14). Nevertheless, the resulting endothelium shows detachment due to the mechanical interactions during stenting and degenerative performance trigged by aggregation of the detached cells.

In contrast, surface bioengineering approaches have shown inherent superiority as they endow the vascular implants with rapid restoration of functional endothelium after implantation in vivo (i.e., in situ endothelialization) (15–19). By incorporating endothelium-specific motifs, vascular implant surfaces can be tailored with desired properties conducive to in situ endothelialization, such as capturing endothelial progenitor cells (EPCs) from the surrounding environment (20–23)(24), and releasing vasoactive mediators to mimic endothelial functions and microenvironments (25, 26). Long-term effects of these endothelium-specific surface engineering strategies are, however, far from ideal due to the complexity of endothelium functions and the monotonicity of surface bioactivity on these vascular implants. In addition, current surface bioengineering strategies mainly rely on chemical conjugation of bioactive molecules; this biomolecule grafting approach will inevitably consume the active groups (e.g., NH_2, SH) of a biomolecule, potentially sacrificing its bioactivity (27, 28). Moreover, these methods mostly involve tedious chemical reactions and sophisticated surface treatments. Apart from potential damage to bioactivity, the complexity of traditional chemical reactions also compromises the controllability, operability, and reproducibility of a multicomponent bioactive surface.

Significance

An ideal metal vascular stent has multiple properties for successful reendothelialization. These properties include 1) inhibiting thrombosis by preventing platelet activation/adhesion, 2) suppressing smooth muscle cell migration/proliferation, and 3) accelerating endothelial cell migration/proliferation. With an easy-to-perform, two-step surface bioengineering approach, the multifunctionalized stents reported here contain two vasoactive moieties (i.e., the nitric-oxide-generating organoselenium and the endothelial progenitor cell-targeting peptide) to satisfy all requirements. The surface engineering strategy presented here can be translated into clinical coatings for cardiovascular stents and will benefit enormously and globally the cardiovascular disease patients; it will, moreover, offer insights to engineering surfaces of blood-contacting devices.

Author contributions: Z.Y., N.H., and G.P. designed research; Z.Y., X.Z., R.H., and Q.T. performed research; Z.Y., X.Z., X.T., Y.X., K.X., M.W., Y.F., N.H., and G.P. analyzed data; and Z.Y., X.Z., and G.P. wrote the paper.

The authors declare no competing interest.

This article is a PNAS Direct Submission.

[1]Z.Y. and X.Z. contributed equally to this work.

[2]To whom correspondence may be addressed. Email: huangnan1956@163.com or panguoqing@ujs.edu.cn.

This article contains supporting information online at https://www.pnas.org/lookup/suppl/doi:10.1073/pnas.2003732117/-/DCSupplemental.

First published June 29, 2020.

Here, we functionalize metal vascular stents in a two-step manner by combining mussel-inspired molecular adhesion and bioorthogonal click chemistry (Scheme 1). First, we coat the stent surfaces with a clickable mussel-inspired peptide with azido (N_3) and catechol groups by mimicking the molecular structure of mussel foot proteins (Mfps) (29, 30). Similar to Mfp adhesion, the mussel-inspired peptide can stably bind onto the metal stents via spontaneous metal–catechol coordination. Afterward, two vasoactive moieties, organoselenium (a glutathione peroxidase-like catalyst capable of decomposing endogenous S-nitrosothiols [RSNOs] into nitric oxide [NO]) (31) and EPC-binding TPS (a human blood outgrowth endothelial cell [HBOEC]-specific peptide for EPC targeting) (32, 33), are modified with N_3-complementary reactive group dibenzylcyclooctyne (DBCO) (34). The surface-bound N_3 groups then enable grafting of DBCO-modified active moieties through bioorthogonal N_3-DBCO click reaction. Due to the specificity, rapidness, and thoroughness of bioorthogonal chemistry (34), vascular stents with tunable dual functions (i.e., NO-generating and EPC-capturing properties) can be readily obtained via a feeding-dependent cografting process. The motivation to use NO-generating compound comes from the antiplatelet aggregation and SMC inhibition capabilities of NO molecules (35–37), and the TPS due to its homing capabilities of circulating blood EPCs, thus accelerating the endothelialization process. This study integrates NO-generating and EPC-capturing moieties into one cardiovascular stent coating system while involving only simple, specific, rapid, and reproducible procedures. This allows for easy mass fabrication and popularization of our cardiovascular coatings. We discover that the SeCA-catalyzed NO generation and TPS-induced EPC capture have contributed synergistically and successfully to in vitro antithrombosis, SMC inhibition, and endothelial cell (EC) promotion. At the optimal SeCA/TPS feeding ratio of 2:2, we observe excellent in vivo endothelialization and ISR prevention. We expect our strategy to provide a facile approach for rational bioengineering of vascular stents with optimal multifunctions. Such vascular stents can tackle

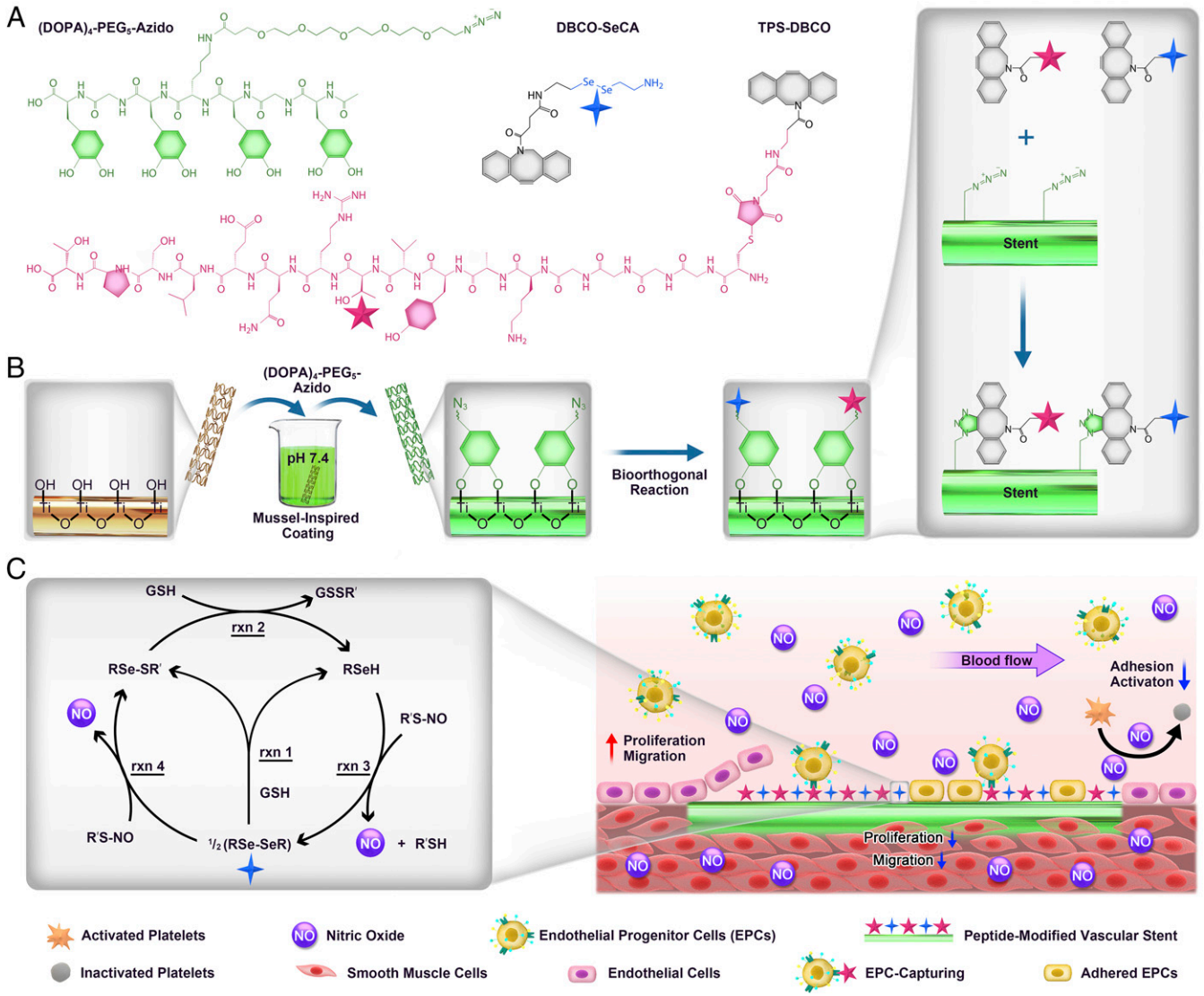

Scheme 1. (*A*) Structural formula of the clickable mussel-inspired peptide [3,4-dihydroxy-L-phenylalanine $(DOPA)_4$-polyethylene glycol (PEG_5)-Azide], NO-generating organoselenium [dibenzylcyclooctyne (DBCO)-SeCA], and EPC-binding peptide (targeting peptide, TPS-DBCO). (*B*) Surface cografting on representative vascular stents through mussel-inspired coordinative interactions and bioorthogonal click chemistry. (*C*) The catalytic reactions of nitric acid (NO) generation process by SeCA and the proposed mechanism of SeCA/TPS cografted stents for antiplatelet adhesion, SMC inhibition, EPC homing, EC growth, and reendothelialization.

the complicated endothelial pathological microenvironments, promote rapid reendothelialization, and ultimately improve clinical outcomes of stenting by reducing the restenosis.

Results

Molecular Synthesis and Surface Functionalization. The clickable mussel-inspired peptide was prepared by solid-phase peptide synthesis according to our previously reported method (38–40). Briefly, DOPA, a catecholic amino acid abundant in Mfps (30, 41), was introduced into the peptide sequence using acetonide-protected Fluorenylmethyloxycarbonyl-DOPA(acetone)-OH. To facilitate the mussellike molecular adhesion onto the metal substrates and leave accessible clickable groups for second-step click reaction, tetravalent DOPA with one amino acid interval and PEG-linked azide were integrated to obtain a clickable mussel-inspired adhesive peptide Ac-(DOPA)-Gly-(DOPA)-(Lys-PEG_5-Azide)-(DOPA)-Gly-(DOPA)-COOH [i.e., $(DOPA)_4$-PEG_5-Azide] (Scheme 1*A*). As two key vasoactive factors for endothelium regeneration, the NO-generating organoselenium (C, SeCA) (31, 42) and EPC-binding TPS (Thr-Pro-Ser-Leu-Glu-Gln-Arg-Thr-Val-Tyr-Ala-Lys) were conjugated with DBCO via *N*-hydroxysuccinimide-amine and maleimide–thiol coupling, respectively (Scheme 1*A*). The obtained DBCO-capped NO catalyst (DBCO-SeCA) and EPC-binding peptide (TPS-DBCO) thus could be easily connected with $(DOPA)_4$-PEG_5-Azide-bound surfaces, which would enable a flexible biofunctionalization (Scheme 1*B*). After purification through high-performance liquid chromatography (HPLC), the three synthesized molecules were then characterized with electrospray ionization mass spectrometry. The monoisotopic mass $[M+H]^+$ of $(DOPA)_4$-PEG_5-Azide, $[M-H]^-$ of DBCO-SeCA, and $[M+2H]^{2+}$ of TPS-DBCO were measured at 1,336.8, 534.1, and 1,077.0 Da, corresponding to their theoretical molecular weight 1,335.6, 535.0, and 2,152.0, respectively (Fig. 1 *A*–*C*). These results demonstrated the successful synthesis of azide-modified mussel adhesive peptide mimic and DBCO-capped endothelial growth factors.

Multivalent catechol-containing molecules could easily and stably bind onto the metal-oxide surfaces through coordination. In this study, we modified the TiO_2-coated 316L stainless steel (SS) with $(DOPA)_4$-PEG_5-Azide. The $(DOPA)_4$-PEG_5-Azide can be strongly chelated to the TiO_2-coated surfaces based on the catecholato-Ti coordinate covalent bond. We used TiO_2-coated 316 L SS (noted as TiO_2 in this study) as a control as TiO_2 coated stents (e.g., HELIOS) are widely used clinically (43), and they have demonstrated improved hemocompatibility, cytocompatibility, and histocompatibility compared to conventional naked 316L SS stents (44). To monitor the peptide binding and biomolecular grafting, we used quartz-crystal microbalance (QCM). As shown in Fig. 1*D*, $(DOPA)_4$-PEG_5-Azide demonstrated steady binding onto the QCM chips and reached up to a

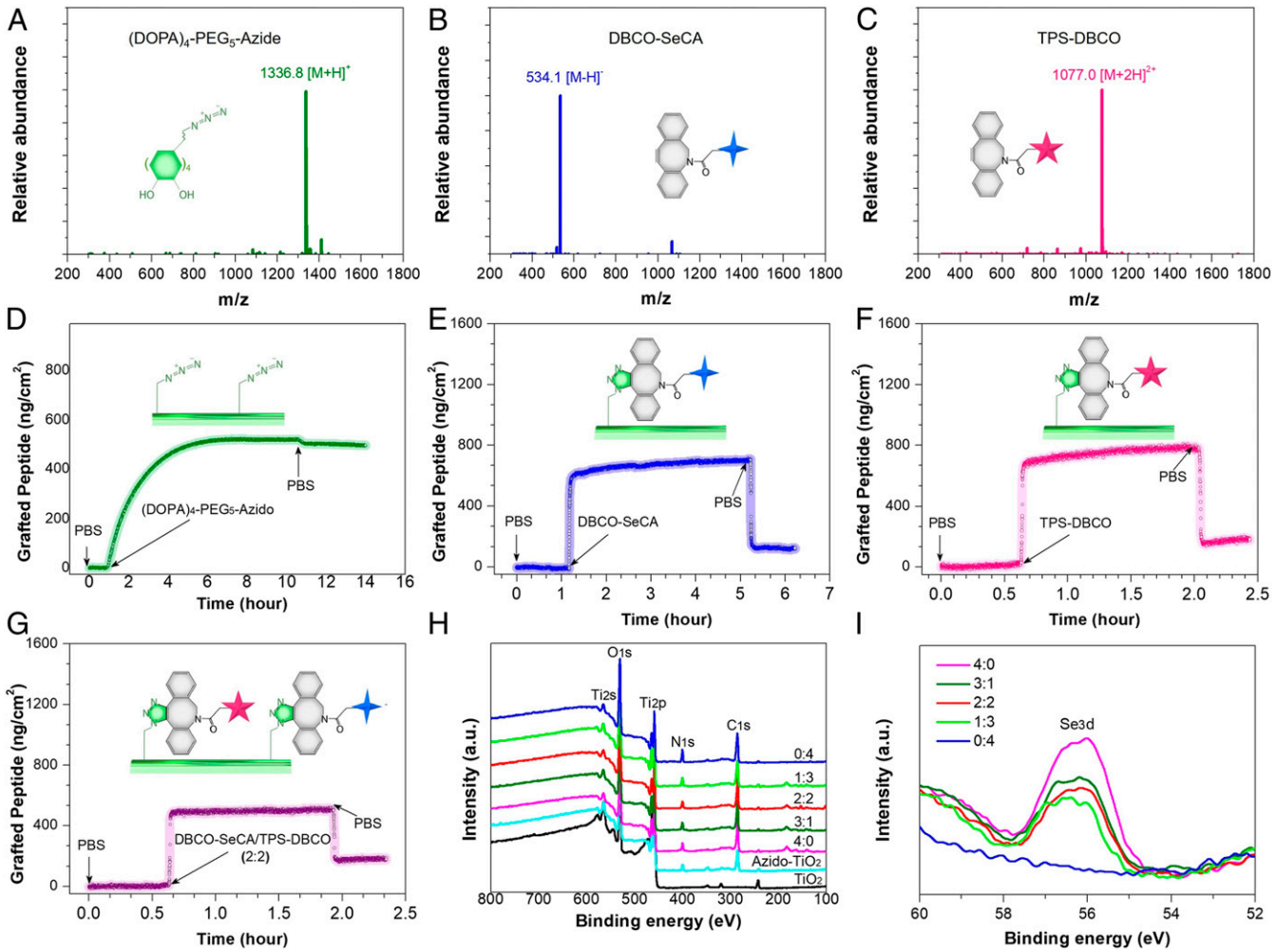

Fig. 1. Electrospray ionization mass spectrum of (*A*) $(DOPA)_4$-PEG_5-Azide, (*B*) DBCO-SeCA, and (*C*) TPS-DBCO. (*D*) Real-time monitoring of the binding of $(DOPA)_4$-PEG_5-Azide on a TiO_2-coated chip determined by QCM. (*E*) DBCO-SeCA, (*F*) TPS-DBCO, and (*G*) DBCO-SeCA/TPS-DBCO cografting process on the $(DOPA)_4$-PEG_5-Azide-bound chips. (H) XPS full spectrum and (*I*) Se3d signal peaks of the grafted surfaces.

maximal binding capacity of 498 ng·cm^{-2} (i.e., 372 pmol·cm^{-2}), indicating the high efficiency and spontaneous adhesion onto TiO_2-coated surfaces. Note that the binding capacity here is higher than that of our previous work (274 pmol·cm^{-2}) (38), probably due to the improved catechol orientation for surface binding. Then, the azide-modified chips (TiO_2-Azide) were incubated with DBCO-SeCA or TPS-DBCO for bioorthogonal conjugation (Fig. 1 *E* and *F*). According to QCM with dissipation monitoring analysis, the grafting processes started in a few minutes, and the maximal grafting amount for DBCO-SeCA and TPS-DBCO were 119 and 181 ng·cm^{-2} (224 and 84 pmol·cm^{-2}), respectively. Because of steric hindrance, not all of the azido groups could be grafted with DBCO-capped molecules, and larger molecules (e.g., TPS-DBCO) resulted in less grafting. Further study on dual functionalization was also performed using a mixture of DBCO-SeCA and TPS-DBCO (2:2 in molar ratio), and the cografting amount showed a median value around 169 ng·cm^{-2} (Fig. 1*G*). Surface elemental compositions with different feeding molar ratios of DBCO-SeCA and TPS-DBCO (i.e., 4:0, 3:1, 2:2, 1:3, and 0:4) were then characterized by X-ray photoelectron spectrum (XPS). As shown in Fig. 1*H*, a gradual enhancement in N 1s signal at 400.12 eV was found on the cografted surfaces with increasing proportion of TPS-DBCO. Likewise, the Se 3d signal weakened as the feeding ratio of DBCO-SeCA decreased (Fig. 1*I*). This result indicated that the bioorthogonal conjugation of a grafted moiety depends on its feeding amount, allowing for optimization and control of surface bioactivities.

In Vitro NO Generation and EPC Capture. For in vitro experiments, we used the commercially available TiO_2-coated 316L SS foil as the material is widely used for vascular stent. NO release was first determined by a real-time chemiluminescent assay (45). Phosphate buffer saline solution (pH 7.4) containing 10 μM L-glutathione, an endogenous reductant for selenol (SeH) generation) and 10 μM *S*-nitrosoglutathione (GSNO, an endogenous NO donor for SeH-catalyzed NO generation) was used to simulate the blood environment. Real-time monitoring of NO flux revealed a SeCA dose-dependent NO generation (Fig. 2*A*). With the decreased proportion of DBCO-SeCA for surface grafting, NO generation slowed down. This result indicated the feasibility of bioorthogonal cografting method for not only efficient SeCA conjugation but also controllable NO generation.

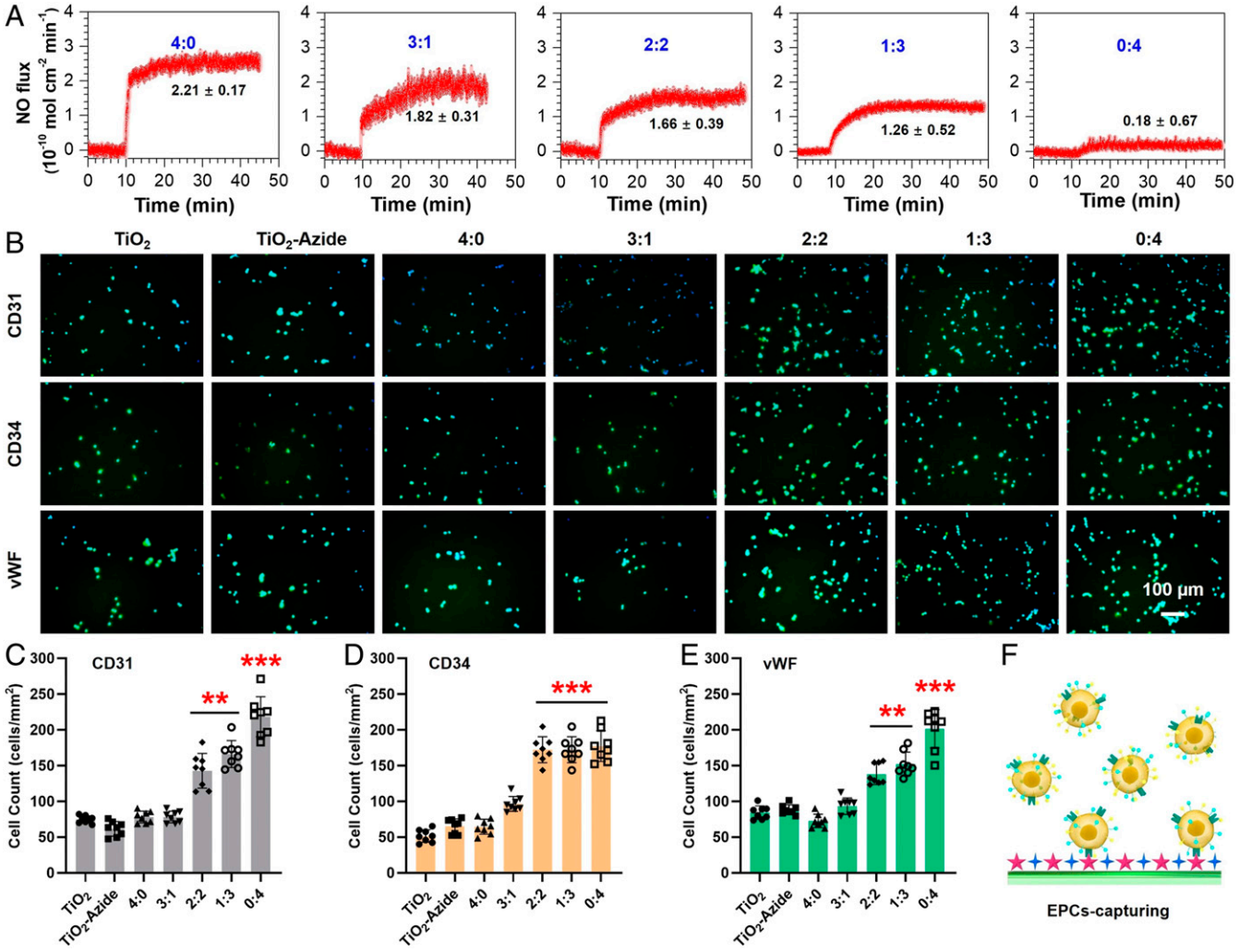

Fig. 2. Effects of SeCA/TPS feeding ratio on NO generation (*A*), EPC capture (*B–E*), and EPC capture mechanism (*F*). (*A*) Rate of NO generation decreased as the SeCA/TPS feeding ratio decreased, indicating a SeCA dose-dependent fashion. (*B*) Endothelial cell markers had higher expressions as the proportion of TPS in the SeCA/TPS increased, demonstrating the EPC-homing abilities of TPS. Quantitative analyses further confirmed the higher adhesion of endothelial cells on the stents by immunostaining of (*C*) CD31, (*D*) CD34, and (*E*) vWF. (*F*) EPCs are captured on the modified stent surface via molecular recognition of TPS.

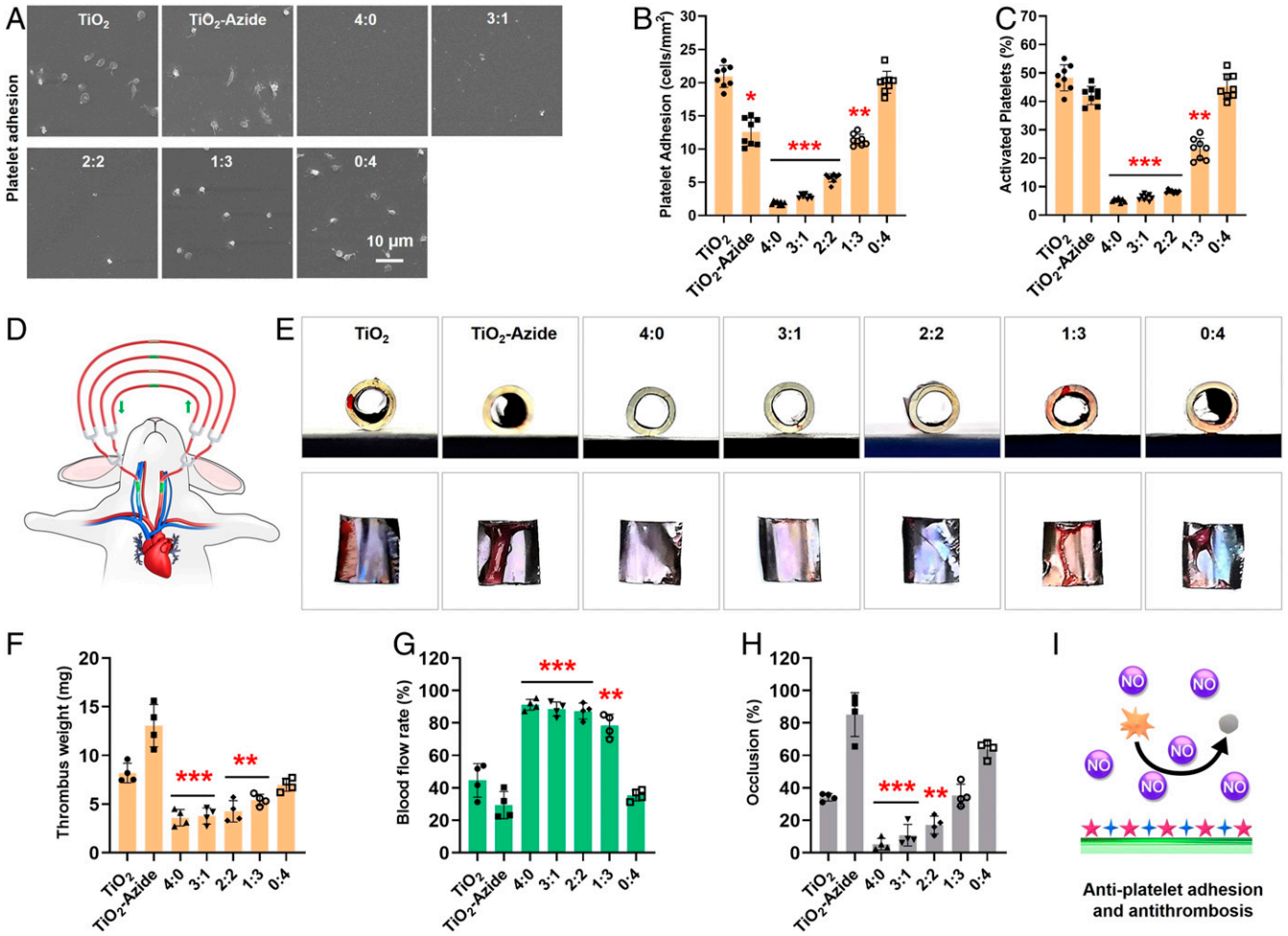

Fig. 3. (*A*) SEM images, (*B*) average density, and (*C*) activation rates of the adhered platelets after incubation with different 316L SS substrates supplemented with NO donor. (*D*) Schematic illustration of the rabbit AV shunt model. (E) Cross-sectional photographs of tubing and the corresponding thrombus formed in different groups. Quantitative results of (*F*) the thrombus weight, (*G*) blood flow, and (*H*) occlusion rate in different groups. (*I*) Schematic antiplatelet adhesion and activation on the cografted surface. Statistically significant differences are indicated by $*P < 0.05$, $**P < 0.005$, $***P < 0.001$ compared with the bare surface (the TiO_2 group).

Another endothelium-related bioactivity is the EPC specificity of TPS. Peripheral blood cultures contain a number of HBOECs, which are a population of late EPCs with endothelial phenotype, high proliferative capacity, and several EC markers, such as CD31, CD34, and von Willebrand factor (vWF) (46). TPS-grafted surfaces in blood environment can induce EPC recognition, adhesion, and proliferation, which would facilitate reendothelialization on vascular stents. To determine the EPC-targeting activity, mesenchymal stem cells were isolated from Danforth's short tail (Sd) mouse for endothelial differentiation into EPCs (*SI Appendix*, Fig. S1). The untreated 316L SS substrates (i.e., TiO_2 group) and $(DOPA)_4$-PEG_5-Azide-treated substrates (TiO_2-Azide group) were used as controls. All substrates were placed in a chamber with a flow of EPC suspension for 2 h (*SI Appendix*, Fig. S2), and the captured cells on different surfaces were stained by immunofluorescence for CD31, CD34, and vWF. As shown in Fig. 2*B*, all of the groups could elicit recognizable EPC adhesion, and the cografted groups with higher TPS-DBCO feeding (e.g., 2:2, 1:3, and 0:4) displayed evidently stronger EPC-capturing activity compared to the others. Quantitative analysis further confirmed this finding (Fig. 2 *C*–*E*). Furthermore, the results also indicated that significantly enhanced EPC capture could only be observed when the TPS-DBCO feeding ratio was higher than 50%.

In Vitro Antiplatelet Adhesion and Ex Vivo Antithrombogenic Properties. At the early stage after implantation, thrombosis on stents is a crucial problem. As a star gaseous signaling molecule, endogenous NO affects a number of cellular processes. In the cardiovascular system, NO can bind to the heme moiety of soluble guanylate cyclase (sGC), leading to sGC activation and subsequent cyclic guanosine monophosphate (cGMP) up-regulation (36, 47). The resultant NO-cGMP signaling and a series of cascades modulate numerous key physiological processes including the prevention of platelet activation and aggregation, inhibition of SMC proliferation, and promotion of EC growth (48). Hence, surface engineering of metal stents with NO-generating property is a bioinspired solution to promote endothelization and to reduce ISR. Here, we first investigated platelet adhesion on the cografted 316L SS substrates. For all in vitro experiments, extra NO donor (GSNO, 10 μM) was used to level the concentrations of RSNOs in physiology. Without donor supply, all groups had substantial platelet adhesion and activation in 30 min, and the grafted groups showed almost no inhibition in the amount and activation rates of adhered platelets

(*SI Appendix*, Fig. S3). Upon adding donor to generate NO, significant changes were observed in the SeCA-containing groups. As shown in Fig. 3*A*, the control groups (TiO_2 and TiO_2-Azide) and the grafted group without SeCA (0:4) still had evident platelet adhesion, and the spread morphology of platelets showed a high degree of activation and aggregation. In contrast, the SeCA-containing groups (4:0, 3:1, 2:2, and 1:3) all showed substantially reduced platelet adhesion with inactive spherical state. Quantitative analysis revealed that only the grafted groups with higher DBCO-SeCA feeding ratios (4:0, 3:1, and 2:2) could significantly inhibit platelet adhesion and activation (Fig. 3 *B* and *C*). Moreover, the inhibitory efficiency showed a DBCO-SeCA feeding-dependent manner, indicating the importance of sufficient SeCA content for platelet inhibition.

We further investigated the antithrombogenic property of our stents using ex vivo perfusion experiments (49). The 316L SS foils with different surface components were curled up and placed onto the inner walls of commercially available cardiopulmonary perfusion tubes, which were then connected to a rabbit arteriovenous shunt (Fig. 3*D*). The ability of the grafted surfaces to support blood flow was evaluated in the presence of NO donor. After 2 h of circulation, the sizes of occlusive thrombosis, thrombus weight, and blood-flow rates in the circuit were evaluated (Fig. 3 *E*–*H*). We found that there was serious thrombus formation on the three SeCA-free control groups (i.e., TiO_2, TiO_2-Azide, and 0:4). On the other hand, only a small number of cruor were observed on the groups with high SeCA contents (i.e., 4:0, 3:1 and 2:2) (Fig. 3*F*). Quantitative analysis further confirmed the above results and demonstrated significant reduction in thrombosis formation of the SeCA-grafted groups with mean thrombosis weight (Fig. 3*F*, 4.26 mg vs. 9.40 mg), blood-flow rate (Fig. 3*G*, 86.34% vs. 36.43%), and occlusion percentage (Fig. 3*H*, 14.73% vs. 61.03%) compared to the SeCA-free controls. The above results have suggested the significance of sufficient SeCA content for efficient antithrombosis.

In Vitro Vascular Cell Growth. In addition to antiplatelet and antithrombotic properties, we also explored the effect of cografted surfaces on SMC inhibition because of its correlation to neointimal hyperplasia. Human umbilical arterial smooth muscle cells (HUASMCs) (*SI Appendix*, Fig. S4) were seeded onto different 316L SS substrates, and the morphology, amount, and proliferation of adhered HUASMCs were characterized by fluorescence staining, counting, and cholecystokinin octapeptide (CCK-8) assay, respectively (Fig. 4 *A* and *B*, and also see *SI Appendix*, Fig. S5). The adhesion and growth of HUASMCs on the SeCA-free groups (TiO_2, TiO_2-Azide, and 0:4) showed no significant difference regardless of whether the medium was supplemented with donor. In contrast, the SeCA-containing groups (4:0, 3:1, 2:2, and 1:3) could efficiently inhibit HUASMC adhesion and proliferation when the medium was supplemented with donor. The result further indicated that, to generate sufficient NO for platelet and SMC inhibition, the feeding ratio of SeCA-DBCO in cografting process should be no less than 50%.

Efficient EC proliferation and migration are another key process to generate endothelium on the implanted stents. Since NO molecule and TPS peptide both could provide EC-friendly microenvironment, human umbilical vein endothelial cells (HUVECs) (*SI Appendix*, Fig. S4) were then used to investigate EC compatibility of the grafted substrates (Fig. 4 *C* and *D*). In this study, HUVECs are used instead of human aortic endothelial cells (HAECs) due to their ready availability and similar cellular characteristics to HAECs in a two-dimensional culture (42, 50–52). We found that, with donor supplement, all grafted groups showed significant enhancement of HUVEC adhesion and proliferation compared with the ungrafted controls. Without

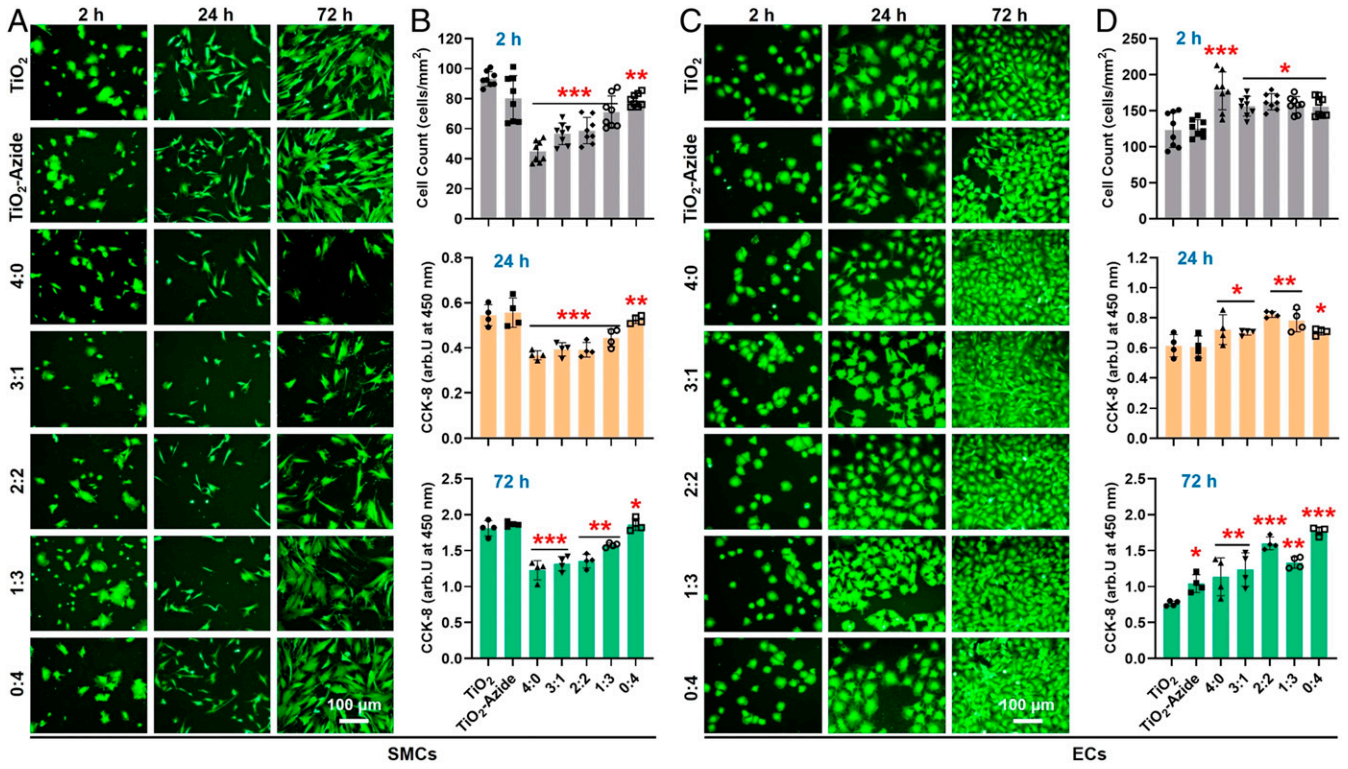

Fig. 4. (*A* and *B*) HUASMC adhesion and proliferation in medium supplemented with NO donor. (*C* and *D*) HUVEC adhesion and proliferation with NO donor supplement. Statistically significant differences are indicated by $*P < 0.05$, $**P < 0.005$, or $***P < 0.001$ compared with the control group.

donor supplement, such enhancement all experienced a certain decrease but still showed significant differences (*SI Appendix*, Fig. S6). These results demonstrated that NO production by SeCA and the EC-TPS binding synergistically promote EC attachment, spreading, and proliferation. Together, our stents showed desirable properties for vascular endothelialization (i.e., the enhancement of EC migration but opposite effects on SMCs).

To confirm this deduction, the migration of these two vascular cells were evaluated and compared. The competitive growth behaviors between HUVECs and HUASMCs on different samples were conducted to deduce the in vivo reendothelialization efficacy of our coatings. We found that in the absence of NO donor, migrations of HUVECs and HUASMCs on all surfaces showed no significant difference (*SI Appendix*, Fig. S7). Upon the addition of donor, cell migration on the NO-generating surfaces (e.g., 4:0, 3:1, and 2:2) changed remarkably (Fig. 5 *A* and *B*). Taking the group of 2:2 for example, cell migration distance showed a decrease of 30.8% for HUASMCs but an increase of 15.0% for HUVECs. Cell migration on the TPS monografted group (i.e., 0:4) showed no changes regardless of donor supplement. These results jointly demonstrated that NO produced by SeCA could provide EC-friendly microenvironment to enhance EC motility and inhibit excessive SMC growth. Such feature is also expected to bring in rapid regeneration of endothelium and reduced neointimal proliferation after vascular stent implantation. However, the ECs compete with SMCs in vivo, in particular, after vascular injury or stenting. To investigate the selectivity of these grafted surfaces for vascular cell growth, coculture (1:1) of HUVECs (green staining) and HUASMCs (red staining) was carried out. As shown in *SI Appendix*, Fig. S8, without donor supplement in culture medium, the cografted groups with high DBCO-TPS feeding ratios could elicit enhanced EC adhesion in the first 2 h, whereas no significant difference was found in all groups after 24 h. This finding, together with the negligible effect of TPS peptide on EC migration, indicated that TPS could only enhance the early EC recognition and adhesion but was irrelevant to the following EC proliferation and migration. After the addition of donor, EC adhesion and proliferation on all of the grafted groups exhibited an overwhelming enhancement against those of SMCs (Fig. 5 *C* and *D*). For example, the ratios of HUVECs to HUASMCs adhered onto the grafted 316L SS substrates all showed a nearly twofold increase than those of the controls, demonstrating their excellent selectivity for EC growth. This beneficial effect on ECs (enhancement) and SMCs (inhibition) may be due to the activation of cGMP expression in the NO-cGMP cell signaling pathway and the selective apoptosis of SMCs (53). The above results justified the feasibility of our strategy to inhibit SMC-caused intimal hyperplasia and to generate a pure in situ endothelium onto an optimized cografted stent surface in vivo.

On the whole, the above experiments indicate that the grafted amounts of SeCA and TPS depend on their ratio during bioorthogonal grafting, and both molecules are blood- and vascular-cell-compatible. On one hand, increased NO generation results in lower thrombosis, attenuated SMC inhibition, and

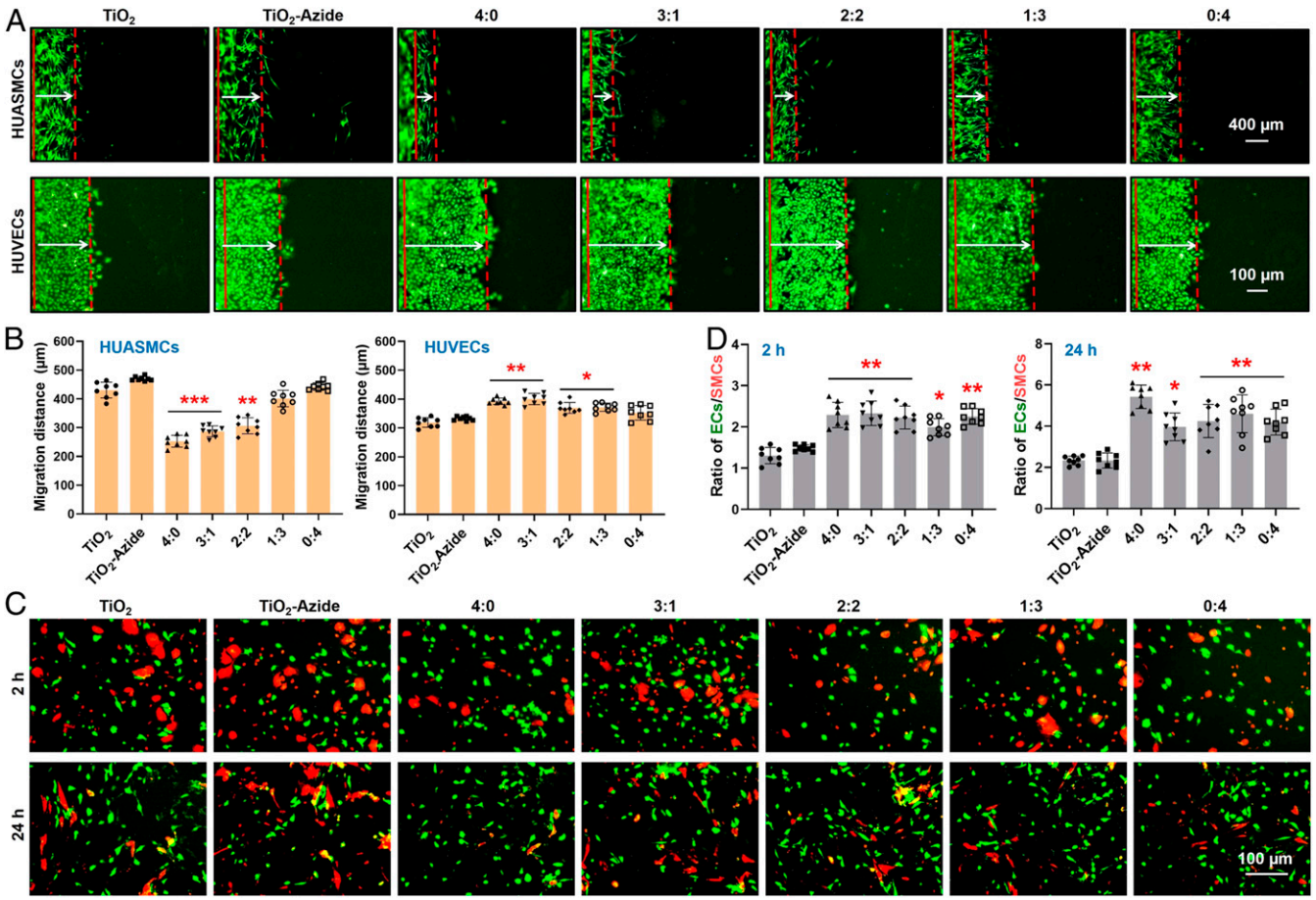

Fig. 5. (*A* and *B*) Migration of HUVECs and HUASMCs on different 316L SS surfaces after 1 d of culture with donor supplement. (*C* and *D*) Competitive growth of HUVECs (green) and HUASMCs (red) on different surfaces with donor supplement. Statistically significant differences are indicated by $*P < 0.05$, $**P < 0.005$, or $***P < 0.001$ compared with the control group.

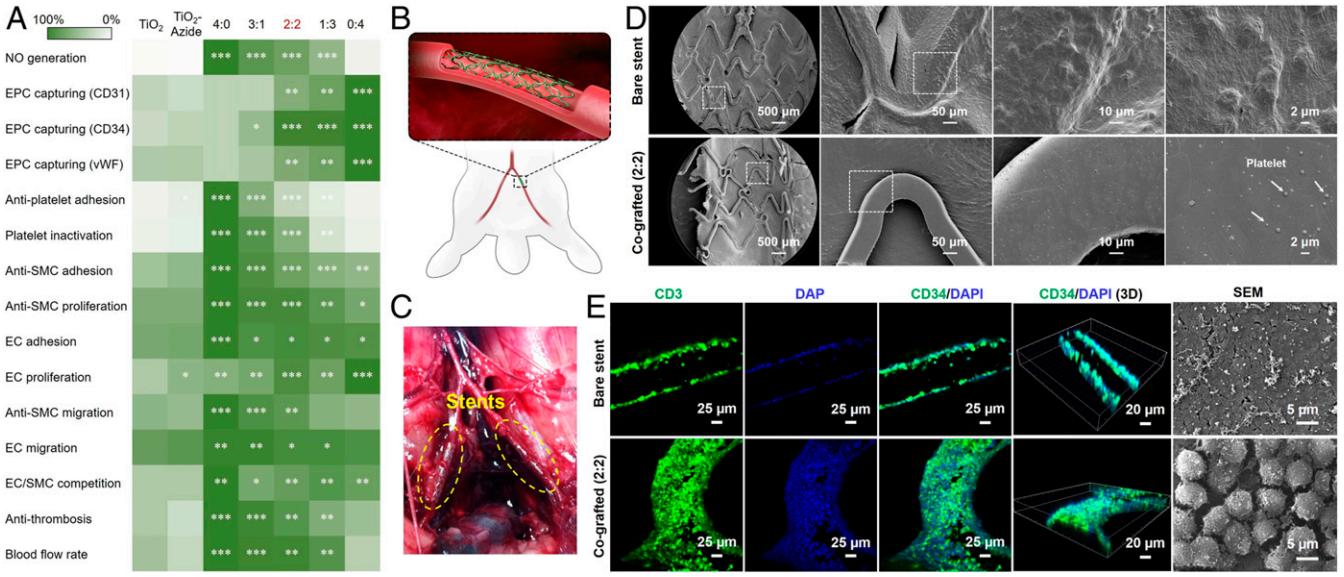

Fig. 6. (*A*) The heat map of vascular-stent-preferred properties. Statistically significant differences are indicated as $*P < 0.05$, $**P < 0.005$, $***P < 0.001$ compared with the control stents. (*B*) Schematic of stent implantation in the iliac arteries of rabbits. (*C*) Experimental photographs of the implanted stents using New Zealand White rabbits. (*D*) Platelet adhesion and (*E*) EPC binding onto the harvested stents after 2 h of implantation.

enhanced EC growth. On the other hand, the increase of EPC-binding peptide on the surfaces facilitates EPC homing and EC growth. To rationally select an optimal cografting condition for vascular stents, all of the in vitro and ex vivo results were summarized in a heat map by normalizing the desired properties of a vascular stent (Fig. 6*A*). The grafted groups with significant differences compared to the control (i.e., the TiO_2 group) were also marked with stars. As clearly shown in the heat map, the cografted surfaces with SeCA/TPS feeding ratio at 2:2 are the most superior, with efficient antithrombosis and SMC inhibition, and excellent EPC binding, EC adhesion, and proliferation. Therefore, this optimized grafting condition was used for subsequent assessment of in vivo efficacy of in situ endothelialization and prevention of restenosis.

In Vivo Anticoagulation and EPC Capture. The ungrafted (control) and cografted (2:2) 316L SS vascular stents were both implanted into the iliac arteries of New Zealand White rabbits with the aid of angiography (Fig. 6 *B* and *C*). Short-term stent implantation (2 h) was first carried out to evaluate blood clotting and EPC capture. As shown in the SEM images (Fig. 6*D*), the control stent surface was covered with a layer of activated platelets and fibrin. In contrast, there was only a small number of scattered and inactivated platelets with spherical shapes on the cografted stent. The result was consistent with those of in vitro antiplatelet adhesion and ex vivo antithrombosis experiments, confirming the early anticoagulant property of the SeCA/TPS cografted stents.

To investigate the practical efficacy for early EPC homing, we further assessed the in vivo EPC capture capacity. The rabbits were injected with granulocyte colony-stimulating factor (G-CSF) to mobilize EPCs into the blood in advance. Two hours after implantation, the stents were harvested and immunostained for CD31, an EC marker highly expressed at endothelial cell–cell junctions (Fig. 6*E*) (54). As expected, the surface of cografted stents showed full green fluorescence, indicating the excellent EPC capture in the first 2 h. On the other hand, the control stent surface showed only nonspecific binding of EPCs, and could not form a confluent cell layer. Similar results with detailed information were also observed in the SEM images of the harvested stents, in which close-arranged EPCs could be found only on the cografted stents. Undoubtedly, the cografted stents showed potent EPC capture capacity for early EPC recruitment, which would facilitate rapid reendothelialization and reduce later neointimal hyperplasia.

In Vivo Reendothelialization and Antirestenosis. Long-term implantation was further performed to demonstrate the potential of the cografted stents for reendothelialization and prevention of ISR. All of the in vivo experiments were carried out with early G-CSF injection for EPC mobilization but without donor supplement. Stented iliac arteries with implanted stents were harvested after 1, 4, and 12 wk of stent deployment. Scanning electron microscope (SEM) images showed that, in the first week, the surface of control stent was fully covered by a thick layer of matrix, whereas the cografted stents still showed clear outline (Fig. 7*A*). Immunostaining revealed that the cografted stents were well-adhered with an intact layer of ECs, but the heavily covered layer on the control stents was partly composed of ECs located just onto the edge of stent skeleton, probably due to the migration of ECs from the surrounding endothelial tissue (Fig. 7*B*). This finding further indicated the excellent and sustained EPC-homing property for early endothelialization in vivo. Given this, the interfacial reendothelialization after 4 and 12 wk of stent implantation was further evaluated. As shown in Fig. 7*C*, although the control stent surface was covered by a layer of cells in weeks 4 and 12, most of the cells were inconsistent with endothelial morphology. Excitingly, the cografted vascular stent was fully covered by an intact EC monolayer, which elongated and aligned to the blood-flow direction under sheared condition. These findings verified that the dual-functional surface with optimized NO generation and EPC capture could significantly promote reendothelialization process on vascular stents.

Histomorphometric analysis was finally performed to examine the effects on preventing intimal hyperplasia and restenosis. After hematoxylin eosin staining, typical cross-sections of arteries with implanted stents were shown in Fig. 7*D*. Clearly, the cografted vascular stents could significantly reduce neointimal hyperplasia during the period of implantation as compared to the control. For example, after 12 wk of implantation, the cografted stents showed remarkable decrease in mean neointimal

stenosis ratio (Fig. 7*E*, 34.4 vs. 20.4%) and mean neointimal area (Fig. 7*F*, 2.43 mm^2 vs. 1.53 mm^2) as compared with the controls. Overall, the cografted vascular stents with optimized NO generation and EPC capture properties could significantly reduce ISR in vivo.

Discussion

Endothelium plays a key role in maintaining cardiovascular homeostasis. To prevent ISR after stenting, timely reendothelialization onto the implanted stents is crucial. However, thrombogenic reaction, aggressive SMC proliferation, and sluggish EC migration at the interfaces of cardiovascular implants are all challenging in reendothelialization. Over the past decades, surface conjugation of endothelium-specific motifs has been widely used to enhance endothelialization. A widely recognized consensus for vascular stent modification is that multifunctional coatings have superiority over the monofunctional ones for tackling the complicated pathological microenvironments. Unfortunately, multicomponent surface functionalization strategies generally suffer from complexity, poor controllability, and low biocompatibility. Hence, we develop a biomimetic method for introducing a multicomponent, bioactive coating onto vascular stent surfaces by combining bioorthogonal conjugation with mussel-inspired adhesive chemistry.

We select two endothelium-specific active moieties, the NO-generating SeCA and the EPC-binding TPS, to optimize the vascular stents. This is because 1) NO is an endogenic signaling molecule capable of inhibition of platelets and SMCs, and 2) TPS enables surface homing of circulating blood EPCs to accelerate endothelialization. The two vasoactive molecules thus include most of the cardiovascular functions of healthy endothelium. To improve

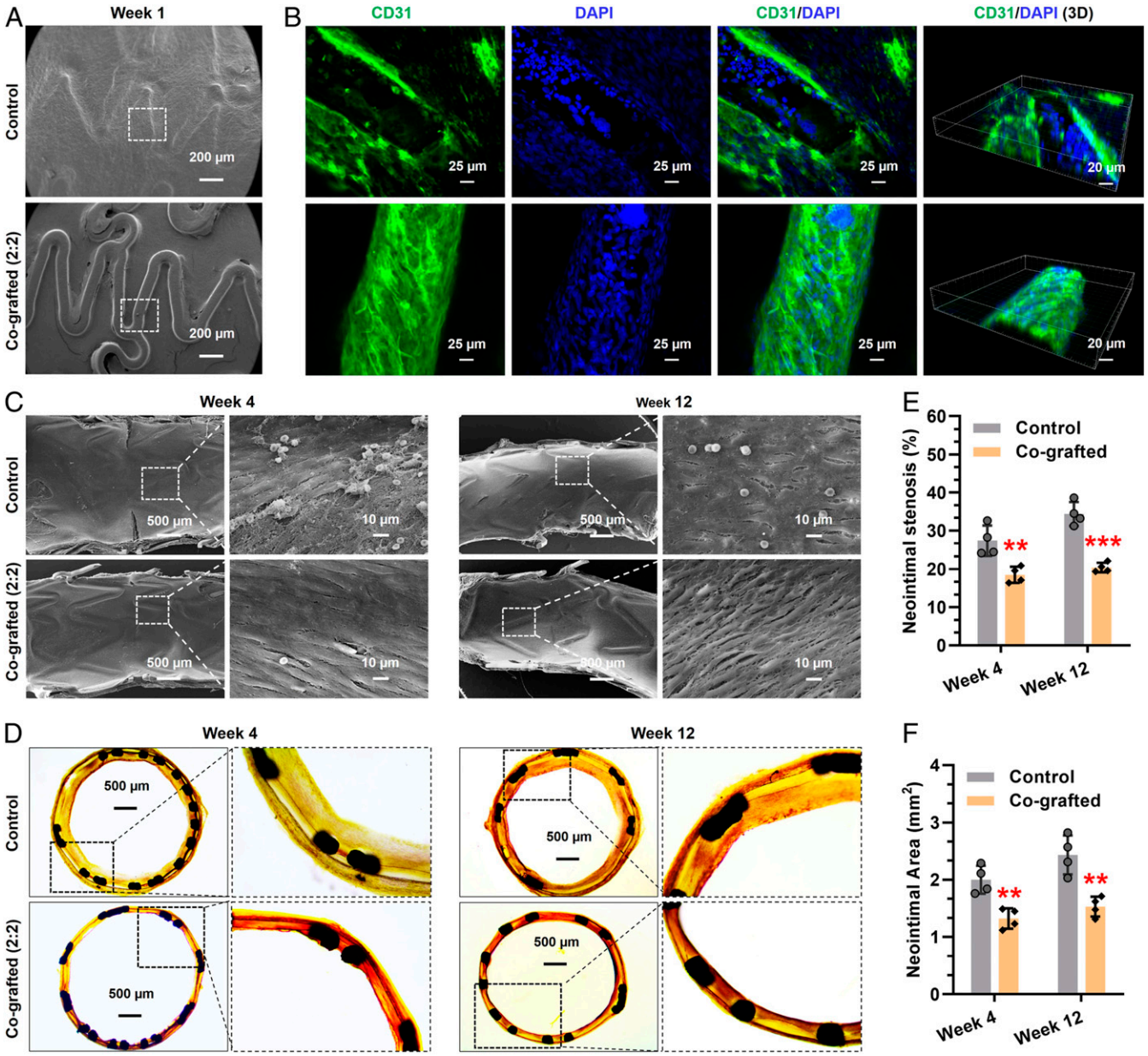

Fig. 7. Long-term stent implantation in vivo. (*A–C*) Re-endothelialization on the control and cografted stents after implantation for 1, 4, and 12 wk. (*D–F*) Histomorphometric and quantitative analysis of ISR prevention in vivo. Statistically significant differences are indicated by $^{**}P < 0.005$, $^{***}P < 0.001$ compared with the control stents.

biocompatibility, mussel-inspired peptide with clickable azido group [$(DOPA)_4$-PEG_5-Azide] was synthesized for the first-step grafting via mussel adhesion mechanism. By modifying SeCA and TPS with DBCO, the two active moieties spontaneously bind onto the mussel-inspired peptide layer through bioorthogonal click chemistry. Compared to traditional chemical means, the combination of mussel adhesion and bioorthogonal chemistry features simplicity, rapidness, and high efficiency: the surface engineering procedure neatly sidesteps tedious reactions and sophisticated surface treatment technologies, reducing the damage toward the tethered bioactive molecules. Moreover, by controlling SeCA/TPS feeding ratio, the cografted surfaces exhibit tunable NO generation, thrombosis and SMC inhibition, excellent EPC capture, EC adhesion and proliferation, efficient reendothelialization, and prevention of ISR. We believe that our surface engineering strategy can be translated into clinical coatings for cardiovascular stents and will benefit enormously and globally the cardiovascular disease patients; it will, furthermore, offer insights to engineering surfaces of blood-contacting devices.

Conclusion

In this work, we integrate multiple desirable functions into one metal vascular stent coating system through the mussel adhesive chemistry and bioorthogonal conjugation. Our SeCA/TPS cografted coating is optimized with different SeCA/TPS feeding ratios and has achieved early antithrombosis, efficient SMC inhibition, potent EPC-capture capacity, rapid reendothelialization, and effective ISR prevention. In addition to the potential for addressing clinical complications of cardiovascular stents, this biomimetic surface bioengineering method also represents a promising strategy for controlling and optimizing multifunctionalization onto surfaces of other biomedical metallic materials.

Materials and Methods

Details of material synthesis, material characterization, cell culture, in vitro, ex vivo, and in vivo tests are described in *SI Appendix*. All procedures for animal experiments were approved by the Animal Care and Use Committee of Southwest Jiaotong University and complied with the Guideline for the Care and Use of Laboratory Animals of the National Institutes of Health (NIH) of China.

Data Availability Statement. All data for the paper are contained in the article and *SI Appendix*.

ACKNOWLEDGMENTS. The authors acknowledge the financial support from the National Natural Science Foundation of China (Grants 31570957, 21875092, 91649204, and 21574091), the International Cooperation Project by Science and Technology Department of Sichuan Province (Grant 2019YFH0103), the Applied Basic Research Project funded by Sichuan Provincial Science and Technology Department (Grant 2017JY0296), the National Key Research and Development Program of China (Grant 2019YFA0112000), the Innovation and Entrepreneurship Program of Jiangsu Province, the "Six Talent Peaks" program of Jiangsu Province (Grant 2018-XCL-013), and the seed projects of Hong Kong Innovation and Technology Support Programme (Grant ITS/065/19).

1. U. Sigwart, J. Puel, V. Mirkovitch, F. Joffre, L. Kappenberger, Intravascular stents to prevent occlusion and restenosis after transluminal angioplasty. *N. Engl. J. Med.* **316**, 701–706 (1987).
2. G. S. Roubin *et al.*, Intracoronary stenting for acute and threatened closure complicating percutaneous transluminal coronary angioplasty. *Circulation* **85**, 916–927 (1992).
3. G. D. Dangas *et al.*, In-stent restenosis in the drug-eluting stent era. *J. Am. Coll. Cardiol.* **56**, 1897–1907 (2010).
4. H. C. Lowe, S. N. Oesterle, L. M. Khachigian, Coronary in-stent restenosis: Current status and future strategies. *J. Am. Coll. Cardiol.* **39**, 183–193 (2002).
5. R. Mehran *et al.*, Angiographic patterns of in-stent restenosis: Classification and implications for long-term outcome. *Circulation* **100**, 1872–1878 (1999).
6. I. De Scheerder *et al.*, Experimental study of thrombogenicity and foreign body reaction induced by heparin-coated coronary stents. *Circulation* **95**, 1549–1553 (1997).
7. G. Tepe *et al.*, Reduced thrombogenicity of nitinol stents–In vitro evaluation of different surface modifications and coatings. *Biomaterials* **27**, 643–650 (2006).
8. R. Kornowski *et al.*, In-stent restenosis: Contributions of inflammatory responses and arterial injury to neointimal hyperplasia. *J. Am. Coll. Cardiol.* **31**, 224–230 (1998).
9. L. Mauri *et al.*, Stent thrombosis in randomized clinical trials of drug-eluting stents. *N. Engl. J. Med.* **356**, 1020–1029 (2007).
10. D. R. Holmes Jr. *et al.*, Stent thrombosis. *J. Am. Coll. Cardiol.* **56**, 1357–1365 (2010).
11. A. C. Newby, A. B. Zaltsman, Molecular mechanisms in intimal hyperplasia. *J. Pathol.* **190**, 300–309 (2000).
12. M. G. Davies, P. O. Hagen, Pathobiology of intimal hyperplasia. *Br. J. Surg.* **81**, 1254–1269 (1994).
13. A. S. Puranik, E. R. Dawson, N. A. Peppas, Recent advances in drug eluting stents. *Int. J. Pharm.* **441**, 665–679 (2013).
14. T. Shirota, H. Yasui, H. Shimokawa, T. Matsuda, Fabrication of endothelial progenitor cell (EPC)-seeded intravascular stent devices and in vitro endothelialization on hybrid vascular tissue. *Biomaterials* **24**, 2295–2302 (2003).
15. M. Avci-Adali, G. Ziemer, H. P. Wendel, Induction of EPC homing on biofunctionalized vascular grafts for rapid in vivo self-endothelialization–A review of current strategies. *Biotechnol. Adv.* **28**, 119–129 (2010).
16. D. Kong *et al.*, Enhanced inhibition of neointimal hyperplasia by genetically engineered endothelial progenitor cells. *Circulation* **109**, 1769–1775 (2004).
17. H. Lan *et al.*, Progress and prospects of endothelial progenitor cell therapy in coronary stent implantation. *J. Biomed. Mater. Res. B Appl. Biomater.* **104**, 1237–1247 (2016).
18. A. de Mel, G. Jell, M. M. Stevens, A. M. Seifalian, Biofunctionalization of biomaterials for accelerated in situ endothelialization: A review. *Biomacromolecules* **9**, 2969–2979 (2008).
19. X. Li *et al.*, Mussel-inspired "built-up" surface chemistry for combining nitric oxide catalytic and vascular cell selective properties. *Biomaterials* **241**, 119904 (2020).
20. S. R. Meyers, P. T. Hamilton, E. B. Walsh, D. J. Kenan, M. W. Grinstaff, Endothelialization of titanium surfaces. *Adv. Mater.* **19**, 2492–2498 (2007).
21. Q. Lin *et al.*, In situ endothelialization of intravascular stents coated with an anti-CD34 antibody functionalized heparin-collagen multilayer. *Biomaterials* **31**, 4017–4025 (2010).
22. C.-H. Wang *et al.*, Late-outgrowth endothelial cells attenuate intimal hyperplasia contributed by mesenchymal stem cells after vascular injury. *Arterioscler. Thromb. Vasc. Biol.* **28**, 54–60 (2008).
23. W. Zheng *et al.*, Endothelialization and patency of RGD-functionalized vascular grafts in a rabbit carotid artery model. *Biomaterials* **33**, 2880–2891 (2012).
24. Y. Cui *et al.*, In situ endothelialization promoted by SEMA4D and CXCL12 for titanium-based biomaterials. *Semin. Thromb. Hemost.* **44**, 70–80 (2018).
25. A. H. Zisch, U. Schenk, J. C. Schense, S. E. Sakiyama-Elbert, J. A. Hubbell, Covalently conjugated VEGF–Fibrin matrices for endothelialization. *J. Control. Release* **72**, 101–113 (2001).
26. M. J. Wissink *et al.*, Improved endothelialization of vascular grafts by local release of growth factor from heparinized collagen matrices. *J. Control. Release* **64**, 103–114 (2000).
27. X. Ren *et al.*, Surface modification and endothelialization of biomaterials as potential scaffolds for vascular tissue engineering applications. *Chem. Soc. Rev.* **44**, 5680–5742 (2015).
28. J. Li, K. Zhang, N. Huang, Engineering cardiovascular implant surfaces to create a vascular endothelial growth microenvironment. *Biotechnol. J.* **12**, 1600401 (2017).
29. Q. Lin *et al.*, Adhesion mechanisms of the mussel foot proteins mfp-1 and mfp-3. *Proc. Natl. Acad. Sci. U.S.A.* **104**, 3782–3786 (2007).
30. H. Lee, N. F. Scherer, P. B. Messersmith, Single-molecule mechanics of mussel adhesion. *Proc. Natl. Acad. Sci. U.S.A.* **103**, 12999–13003 (2006).
31. W. Cha, M. E. Meyerhoff, Catalytic generation of nitric oxide from S-nitrosothiols using immobilized organoselenium species. *Biomaterials* **28**, 19–27 (2007).
32. A. N. Veleva, S. L. Cooper, C. Patterson, Selection and initial characterization of novel peptide ligands that bind specifically to human blood outgrowth endothelial cells. *Biotechnol. Bioeng.* **98**, 306–312 (2007).
33. A. N. Veleva, D. E. Heath, S. L. Cooper, C. Patterson, Selective endothelial cell attachment to peptide-modified terpolymers. *Biomaterials* **29**, 3656–3661 (2008).
34. D. M. Patterson, J. A. Prescher, Orthogonal bioorthogonal chemistries. *Curr. Opin. Chem. Biol.* **28**, 141–149 (2015).
35. S. S. Ahanchi, N. D. Tsihlis, M. R. Kibbe, The role of nitric oxide in the pathophysiology of intimal hyperplasia. *J. Vasc. Surg.* **45** (suppl. A), A64–A73 (2007).
36. N. Naghavi, A. de Mel, O. S. Alavijeh, B. G. Cousins, A. M. Seifalian, Nitric oxide donors for cardiovascular implant applications. *Small* **9**, 22–35 (2013).
37. M. A. Elnaggar *et al.*, Nitric oxide releasing coronary stent: A new approach using layer-by-layer coating and liposomal encapsulation. *Small* **12**, 6012–6023 (2016).
38. G. Pan *et al.*, Biomimetic design of mussel-derived bioactive peptides for dual-functionalization of titanium-based biomaterials. *J. Am. Chem. Soc.* **138**, 15078–15086 (2016).
39. Y. Ma *et al.*, Mussel-derived, cancer-targeting peptide as pH-sensitive prodrug nanocarrier. *ACS Appl. Mater. Interfaces* **11**, 23948–23956 (2019).
40. L. Liu *et al.*, A versatile dynamic mussel-inspired biointerface: From specific cell behavior modulation to selective cell isolation. *Angew. Chem. Int. Ed. Engl.* **57**, 7878–7882 (2018).
41. T. K. Das *et al.*, In-situ synthesis of magnetic nanoparticle immobilized heterogeneous catalyst through mussel mimetic approach for the efficient removal of water pollutants. *Colloid Interface Sci. Commun.* **33**, 100218 (2019).

42. Z. Yang *et al*., Metal-phenolic surfaces for generating therapeutic nitric oxide gas. *Chem. Mater.* **30**, 5220–5226 (2018).
43. J. Li, S. De Rosa, J. Wang, K. Zhang, Biomaterials development, modification, and potential application for interventional cardiology. *BioMed Res. Int.* **2020**, 4890483 (2020).
44. X. Xu, L. Wang, G. Wang, Y. Jin, The effect of REDV/TiO_2 coating coronary stents on in-stent restenosis and re-endothelialization. *J. Biomater. Appl.* **31**, 911–922 (2017).
45. F. Zhang *et al*., Mussel-inspired dopamine-Cu^{II} coatings for sustained in situ generation of nitric oxide for prevention of stent thrombosis and restenosis. *Biomaterials* **194**, 117–129 (2019).
46. J. Z. He *et al*., Enhanced translation of heme oxygenase-2 preserves human endothelial cell viability during hypoxia. *J. Biol. Chem.* **285**, 9452–9461 (2010).
47. E. Martin, V. Berka, A. L. Tsai, F. Murad, Soluble guanylyl cyclase: The nitric oxide receptor. *Methods Enzymol.* **396**, 478–492 (2005).
48. H. Qiu *et al*., Biomimetic engineering endothelium-like coating on cardiovascular stent through heparin and nitric oxide-generating compound synergistic modification strategy. *Biomaterials* **207**, 10–22 (2019).
49. Y. Yang *et al*., Endothelium-mimicking multifunctional coating modified cardiovascular stents via a stepwise metal-catechol-(amine) surface engineering strategy. *Research (Wash D C)* **2020**, 9203906 (2020).
50. H.-R. Seo *et al*., Intrinsic FGF2 and FGF5 promotes angiogenesis of human aortic endothelial cells in 3D microfluidic angiogenesis system. *Sci. Rep.* **6**, 28832 (2016).
51. Y. Wei *et al*., Surface engineering of cardiovascular stent with endothelial cell selectivity for in vivo re-endothelialisation. *Biomaterials* **34**, 2588–2599 (2013).
52. D. J. Medina-Leyte, M. Domínguez-Pérez, I. Mercado, M. T. Villarreal-Molina, L. Jacobo-Albavera, Use of human umbilical vein endothelial cells (HUVEC) as a model to study cardiovascular disease: A review. *Appl. Sci.* **10**, 938 (2020).
53. T. L. Cornwell, E. Arnold, N. J. Boerth, T. M. Lincoln, Inhibition of smooth muscle cell growth by nitric oxide and activation of cAMP-dependent protein kinase by cGMP. *Am. J. Physiol.* **267**, C1405–C1413 (1994).
54. P. Lertkiatmongkol, D. Liao, H. Mei, Y. Hu, P. J. Newman, Endothelial functions of platelet/endothelial cell adhesion molecule-1 (CD31). *Curr. Opin. Hematol.* **23**, 253–259 (2016).